Exergy analysis of parabolic trough solar collectors integrated with combined steam and organic Rankine cycles

CrossMark

Fahad A. Al-Sulaiman

Mechanical Engineering Department, King Fahd University of Petroleum and Minerals (KFUPM), Dhahran 31261, Saudi Arabia

ABSTRACT

In this paper, detailed exergy analysis of selected thermal power systems driven by parabolic trough solar collectors (PTSCs) is presented. The power is produced using either a steam Rankine cycle (SRC) or a combined cycle, in which the SRC is the topping cycle and an organic Rankine cycle (ORC) is the bottoming cycle. Seven refrigerants for the ORC were examined: R134a, R152a, R290, R407c, R600, R600a, and ammonia. Key exergetic parameters were examined: exergetic efficiency, exergy destruction rate, fuel depletion ratio, irreversibility ratio, and improvement potential. For all the cases considered it was revealed that as the solar irradiation increases, the exergetic efficiency increases. Among the combined cycles examined, the R134a combined cycle demonstrates the best exergetic performance with a maximum exergetic efficiency of 26% followed by the R152a combined cycle with an exergetic efficiency of 25%. Alternatively, the R600a combined cycle has the lowest exergetic efficiency, 20–21%. This study reveals that the main source of exergy destruction is the solar collector where more than 50% of inlet exergy is destructed, or in other words more than 70% of the total destructed exergy. In addition, more than 13% of the inlet exergy is destructed in the evaporator which is equivalent to around 19% of the destructed exergy. Finally, this study reveals that there is an exergetic improvement potential of 75% in the systems considered.

© 2013 Elsevier Ltd. All rights reserved.

1. Introduction

Utilization of solar energy has become crucial and it is expected to increase significantly in the near future. Therefore, there is a need to improve the performance of thermal power plants integrated with solar thermal energy. Parabolic trough solar collector (PTSC) technology is considered the most established solar thermal technology for power production. It has been used in large power plants since the 1980s in California and has demonstrated a promising renewable energy technology for the future. Hence, this technology has been selected for this study.

A number of papers had examined ORCs integrated with PTSCs for electrical power production, e.g. [1–6]. He et al. [1] considered three organic working fluids, R113, R123, and pentane, for an ORC and found that pentane had the best performance. In another study, Quoilin et al. [2] carried out thermodynamic modeling of a proposed small scale PTSC integrated with an ORC for power production, considering different design options to be located in a rural location in Berea District of Lesotho, South Africa. In a different paper, Bamgbopa and Uzgoren [3] developed a transient model for a simple ORC in which the working fluid was R245fa and found

that the heat exchanger was the critical part of the model. In a different study, the performance of a low temperature solar thermal electric system using an ORC and a compound parabolic trough was examined by Gang et al. [4]. It was shown that the overall electrical efficiency was about 8.6% when a solar irradiation of 750 W/m² was assumed. They further examined their system for selected cities and considered an improved design of the oil and organic fluid heat exchanger [5]. Derscha et al. [6] carried out a study that compared the performance of integrated solar combined cycle systems (ISCCs) with a solar electric generating system (SEGS) and found that ISCCs provided a better option than SEGS.

A few studies considered integrating ORC with PTSC for cogeneration or trigeneration, e.g. [7–13].

Li et al. [7] assessed the performance of their system for both power and water production through reverse osmosis (RO) and their system had efficiency between 18% and 20%. In a different study, Nafey and Sharaf [8] conducted thermodynamic analysis for both power and water desalination using RO. They selected four refrigerants for the PTSC case: dodecane, nonane, octane, and toluene and found that toluene was the best option. In another study, Sharaf et al. [9] conducted thermo-economic analysis of PTSC integrated with an ORC and a multi-effect distillation. Two scenarios of generation were considered in their study: the first one was with only water production and the second one was with both power

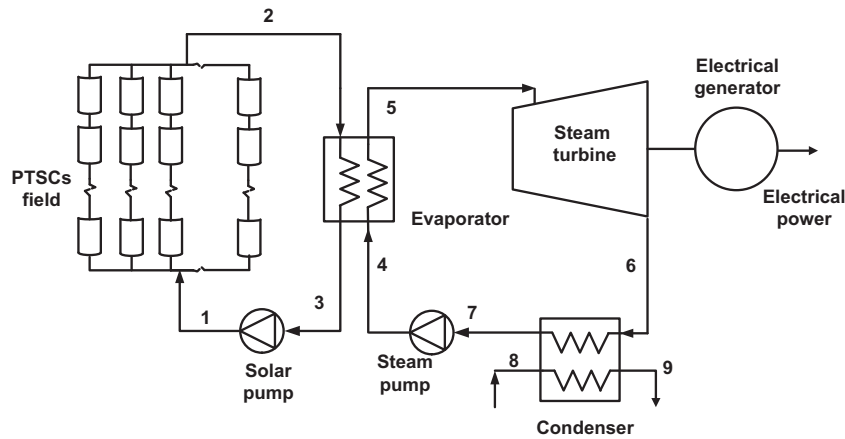*E-mail address:* fahadas@kfupm.edu.sa

Nomenclature

A_{ap}	aperture area, m^2
A_c	area of the receiver cover, m^2
A_r	area of the receiver, m^2
Cp	specific heat, kJ/kg K
Col_s	total number of solar modules per single row (in series)
Col_r	total number of solar collectors rows
D	diameter, m
ex	specific exergy, kJ/kg
Ex	exergy, kW
Ex_d	exergy destruction, kW
F_R	heat removal factor
F_1	collector efficiency factor
G_b	solar radiation intensity, W/m^2
h	enthalpy, kJ/kg
HTF	heat transfer fluid
h_c	convection heat coefficient, kW/m^2 K
h_r	radiation heat coefficient, kW/m^2 K
IP	exergetic improvement potential, kW
k	thermal conductivity, kW/m
$\dot{m}_r$	mass flow rate through the receivers in one row, kg/s
$\dot{m}_{rt}$	total mass flow rate though all receivers in parallel, kg/s
$\dot{m}_{st}$	mass flow rate in the steam Rankine cycle, kg/s
Nus	Nusselt number
ORC	organic Rankine cycle
P	pressure, kPa
Pv	vapor pressure, kPa
$\dot{Q}$	heat rate, kW
$\dot{Q}_{u,o}$	overall useful heat rate through all the collectors, kW
S	entropy, kJ/kg
SRC	steam Rankine cycle
SRC-A	steam Rankine cycle with atmospheric condensing pressure
SRC-V	steam Rankine cycle with vacuum condensing pressure
T	temperature, K
T_s	temperature of the sun, K
U_o	overall heat loss coefficient, kW/K

U_L	solar collector heat loss coefficient between the ambient and receiver, kW/K
v	velocity, m/s
w	collector width, m
Y_D	exergetic fuel depletion ratio
Y_D^*	irreversibility ratio
z	height (elevation), m

Greek letters

α	absorbance of the receiver
η	efficiency
ϵ_{cv}	emittance of the receiver cover
ϵ_r	emittance of the receiver
γ	intercept factor
K_γ	incidence angle modifier
σ	Stefan–Boltzmann constant, kW/m^2 K^4
ρ_c	reflectance of the mirror
τ	transmittance of the glass cover

Subscripts

0	atmospheric conditions
d	destruction
el	electrical power
ev	evaporator
ex	exergy
g	generator
i	inlet
j	property value at state j
o	organic
op	ORC pump
ot	ORC turbine
r	receiver
rt	all the receivers (collectors in parallel)
st	steam
u	useful

and water production. It was found that the first option is more attractive. Delgado-Torres and García-Rodríguez [10,11] conducted thermodynamic analysis of a thermal system consists of an ORC, a PTSC, and an RO. Initially, they analyzed the system assuming only water production through RO [10] and then they extended their study to include both electrical and water production [11]. The main objective of their study [11] was to examine the effect of different organic fluids on the aperture area of the PTSC. In another study, the energetic performance of PTSC integrated with an ORC in which the waste heat from the ORC is used for cogeneration was conducted by Al-Sulaiman et al. [12]. It was found that there was an energy efficiency improvement, when trigeneration was used, from 15% to 94% (utilization efficiency). On the other hand, using exergy analysis, Al-Sulaiman et al. [13] found that there was an exergetic efficiency improvement from 8% to 20% when trigeneration is used as compared to only power generation. Al-Sulaiman [14] conducted energy analysis of PTSC integrated with a steam Rankine cycle as a topping cycle and an ORC as a bottoming cycle. His study considered the energetic performance of his system and the effect of selected parameters on the size of the solar collector field.

It can be observed from the literature review that there is no exergy analysis that has been conducted on parabolic trough solar collectors integrated with combined steam and organic Rankine cycles. Furthermore, with fossil fuel depletion and significant

increment of CO_2 emissions, finding an improved thermal power system driven by a renewable energy, such as solar energy, is becoming more crucial. Therefore, the current study is original and of significant importance. The objective of the current study is to examine, in detail, the exergetic performance of a thermal power system driven by parabolic trough solar collectors that are integrated with combined steam and organic Rankine cycles. The steam Rankine cycle (SRC) is the topping cycle while the ORC is the bottoming cycle. Severn refrigerants for the ORC were considered: R134a, R152a, R290, R407c, R600, R600a, and ammonia. In this study, key exergetic parameters are examined: exergetic efficiency, exergy destruction rate, fuel depletion ratio, irreversibility ratio, and improvement potential.

2. System descriptions

The current study considers two systems. The first one is a PTSC integrated with an SRC, as shown in Fig. 1. Two operating conditions were considered for this system: vacuum condensing pressure and atmospheric condensing pressure. The second system is a combined vapor cycle, which is similar to the first; however, an ORC, as a bottoming cycle, is integrated with SRC that has condensing atmospheric pressure (SRC-A), as a topping cycle, as shown in Fig. 2. The ORC is integrated with an SRC-A since there is a

Fig. 1. Schematic of the parabolic trough solar collectors integrated with steam Rankine cycle.
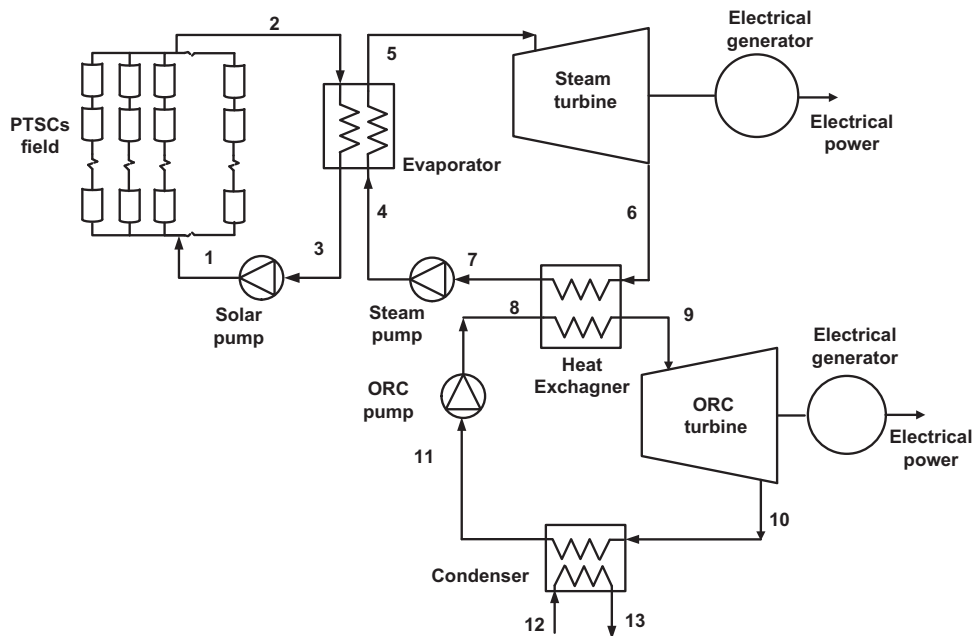

Fig. 2. Schematic of the parabolic trough solar collectors integrated with the steam and organic Rankine cycles.

sufficient amount of waste heat that can be utilized from this SRC-A, unlike the case with an SRC operating under vacuum condensing pressure (SRC-V). Moreover, the combined cycles examined in this study, have another two major advantages as compared to the SRC-V. The SRC-V design is relatively complex because: (a) The pressure in the condenser is at vacuum and, consequently, the capital and operating & maintenance costs are relatively high; which is not the case for the combined cycles; (b) The specific volume of the steam in the condenser is high (SRC-V) and, hence, the SRC-V requires a relatively large condenser while the SRC-A does not. Furthermore, the combined cycle requires another cycle that adds cost. The other two SRCs in this study, SRC-V and SRC-A, are considered as a reference for the combined vapor cycle for comparison.

The solar collector field consists of a few hundred solar collector rows. Each collector row consists of ten modules. The length of each module is 12.27 m [15,16]. Table 1 lists the geometric data of the solar collectors selected. The LS-3 collector type was selected in this study, because it is the latest collector design in SEGS plants, and has proven performance in the field. The temperature at the

exit of the solar collector row is 390 °C (663 K) [17]. This temperature is considered the maximum practical operating temperature of the selected oil that is circulated through the receivers of the PTSC. The oil selected is Thermonil-VP1. It is a synthetic oil that has both good heat transfer properties and good temperature control [18]. Therefore, it is used in many power plants driven by PTSC, [15,19] and, consequently, it has been selected for this study. The thermodynamic characteristics of this oil can be found at [18]. The mass flow rate of the HTF per single row of solar collectors is 0.35–0.8 kg/s [20]. It should be noted that this mass flow rate is for a single solar collector row without looping.

The SRC examined is integrated with the solar field through an evaporator. The pinch point temperature of the evaporator was assumed to be 10 K [21]. For the combined vapor cycle, seven refrigerants were selected. These refrigerants were R134a, R152a, R290, R407c, R600, R600a, and ammonia. They were selected based on the recommendation of Tchanche et al. [22], in which they have recommended these refrigerants for a low temperature ORC, like the case for the bottoming cycle in the combined vapor cycles considered.

Table 1
Input values to the system.

Steam and Rankine cycles	
Steam and ORC turbine efficiency	85%
Steam and ORC pump efficiency	80%
Baseline mass flow rate of the steam Rankine cycle	94 kg/s
Baseline steam turbine inlet pressure	12.0 MPa
Baseline steam turbine inlet temperature	663 K
Pinch point temperature of the evaporator/condenser	10 K
Electrical generator efficiency	96%
Electrical motor efficiency	96%
Solar collectors [16,27]	
Single collector width	5.76 m
Single collector length	12.27 m
Receiver inner diameter	0.066 m
Receiver outer diameter	0.07 m
Cover inner diameter	0.115 m
Cover outer diameter	0.121 m
Emittance of the cover	0.86
Emittance of the receiver	0.15
Reflectance of the mirror	0.94
Intercept factor	0.93
Transmittance of the glass cover	0.96
Absorbance of the receiver	0.96
Incidence angle modifier	1
Number of collectors in series	10
Ambient conditions	
Ambient temperature	298.15 K
Ambient pressure	101.3 kPa

3. Mathematical modeling

Mathematical modeling of the systems considered is presented in this section. The equations developed were programmed using Engineering Equation Solver (EES). The input data used in the code are listed in Table 1. Modeling of the PTSC in this section is based on the equations presented in [23,24]. The developed equations were validated with these two references and with the experimental study by Dudley et al. [25]. The validation is presented later in this section.

Modeling the solar system is presented first. Then the exergy analysis of the overall system is presented. It was assumed that the systems are at steady state. In addition, it was assumed that the pressure change is negligible except in the pumps and turbines. The useful collected energy rate from a single collector is defined as:

$$\dot{Q}_u = \dot{m}_r(Cp_{ro}T_{ro} - Cp_{ri}T_{ri}) \tag{1}$$

where Cp is the specific heat, $\dot{m}_r$ is the mass flow rate in the receiver, and T is the temperature. The subscripts *ro* and *ri* refer to the receiver inlet and the receiver outlet, respectively. This useful energy can also be calculated from:

$$\dot{Q}_u = A_{ap}F_R\left(S - \frac{A_r}{A_{ap}}U_L(T_{ri} - T_0)\right) \tag{2}$$

where F_R is the heat removal factor, S is the heat absorbed by the receiver, A_{ap} is the aperture area, A_r is the receiver area, and U_L is the solar collector overall heat loss coefficient. The heat absorbed by the receiver is defined as:

$$S = G_b\eta_r \tag{3}$$

where G_b is the direct irradiation intensity and η_r is the receiver efficiency which is defined as [17]:

$$\eta_r = \rho_c\gamma\tau\alpha\, K_\gamma \tag{4}$$

where ρ_c, γ, τ, α and K_γ are the reflectance of the mirror, intercept factor, transmittance of the glass cover, absorbance of the receiver, and incidence angle modifier, respectively; their values are listed in Table 1. The heat removal factor is defined as:

$$F_R = \frac{\dot{m}_r Cp_r}{A_r U_L}\left[1 - \exp\left(\frac{-A_r U_L F_1}{\dot{m}_r Cp_r}\right)\right] \tag{5}$$

where $\dot{m}_r$ is the mass flow rate through the receiver and F_1 is the collector efficiency factor and defined as:

$$F_1 = U_o/U_L \tag{6}$$

The solar collector heat loss coefficient between ambient and receiver is defined as:

$$U_L = \left[\frac{A_r}{(h_{c,ca} + h_{r,ca})A_c} + \frac{1}{h_{r,cr}}\right]^{-1} \tag{7}$$

The radiation heat coefficient between ambient and the cover is defined as:

$$h_{r,ca} = \epsilon_{cv}\sigma(T_c + T_a)(T_c^2 + T_a^2) \tag{8}$$

where σ is Stefan–Boltzmann constant and ϵ_{cv} is the emittance of the cover. The radiation heat coefficient between the cover and the receiver is defined as:

$$h_{r,cr} = \frac{\sigma(T_c + T_{r,av})(T_c^2 + T_{r,av}^2)}{\frac{1}{\epsilon_r} + \frac{A_r}{A_c}\left(\frac{1}{\epsilon_{cv}} - 1\right)} \tag{9}$$

where the subscript *av* refers to average and ϵ_r is the emittance of the receiver. The convection heat loss coefficient between ambient and the cover is defined as:

$$h_{c,ca} = \left(\frac{Nus\, k_{air}}{D_{c,o}}\right) \tag{10}$$

where K_{air} is the thermal conductivity of the air and Nus is Nusselt number. The overall heat coefficient between the surroundings and the fluid is defined as:

$$U_o = \left[\frac{1}{U_L} + \frac{D_{r,o}}{h_{c,r,in}D_{r,i}} + \left(\frac{D_{r,o}}{2k_r}\ln\left(\frac{D_{r,o}}{D_{r,i}}\right)\right)\right]^{-1} \tag{11}$$

where $h_{c,r,in}$ is the heat loss coefficient between the receiver and the cover which is defined as:

$$h_{c,r,in} = \frac{Nus_r k_r}{D_{r,i}} \tag{12}$$

The subscript *r* refers to the receiver. The temperature of the cover can be calculated using this equation:

$$T_c = \frac{h_{r,cr}T_{r,a} + \frac{A_c}{A_r}(h_{c,ca} + h_{r,ca})T_0}{h_{r,cr} + \frac{A_c}{A_r}(h_{c,ca} + h_{r,ca})} \tag{13}$$

The amount of the solar irradiation that shines upon the collector, which is considered as heat into the system, is defined as:

$$\dot{Q}_{solar} = A_{ap}F_R S Col_r Col_s \tag{14}$$

where Col_s and Col_r are the total number of modules in series and the total number of the collector rows (parallel). The aperture area is defined as:

Table 2
Validation of the current model as compared with Dudley et al. [25]. Heat losses change with the average temperature above the ambient of the fluid inside the absorber.

$Ta,_{am}$ difference	Heat loss (Model)	Heat loss (Exp. [26])
100.6	8.7	10.6
149.1	19.3	19.3
196.7	34.2	30.6
245.8	53	45.4
293.3	75.5	62.9

$$A_{ap} = (w - D_{co})L \tag{15}$$

where L, w, and D_{co} are the collector (module) length, collector width, and receiver cover outer diameter, respectively. The validation of the PTSC model is presented next.

The solar collector model is validated against the experimental study by Dudley et al. [25], as shown in Table 2. The model demonstrates good agreement with the experimental work. The small deviation in the current model as compared to [25] is due mainly to the approximation used to calculate the heat loss coefficients.

Exergy is a measure of the departure of a state of a system from that of the surroundings. It is defined as the maximum theoretical work that can be attained from a system as it interacts with the equilibrium state (surroundings). The exergy balance of a control volume at steady state can be defined as:

$$0 = \sum_j \left(1 - \frac{T_o}{T_j}\right)\dot{Q}_j - \dot{W}_{cv} + \sum_i \dot{m}_i ex_i - \sum_e \dot{m}_e ex_e - \dot{Ex}_d \tag{16}$$

where $\dot{E}_{x_d}$, ex, and T are the exergy destruction rate, exergy per unit mass flow rate, and temperature, respectively. The subscript 0 is the value of the property at the surrounding and the subscript j is the property value at state j. The subscripts i and e refer to the inlet and exit, respectively. The physical exergy per mass flow rate, ex^{ph}, at a given state is defined as [17]:

$$ex^{ph} = (h - h_0) - T_0(s - s_0) + \left(\frac{V^2 - V_0^2}{2}\right) + g(z - z_0) \tag{17}$$

where h, s, v, g, and z are enthalpy per unit mass, entropy per unit mass, velocity, gravity, and elevation, respectively. In this study, the elevation and velocity are neglected because they are significantly small as compared to the other values.

The exergy efficiency is defined as the ratio of the actual thermal efficiency to the maximum reversible thermal efficiency in which both are under the same conditions. The net electrical exergy efficiency is defined as:

$$\eta_{ex,el} = \frac{\dot{W}_{net}}{Ex_{in}} \tag{18}$$

where Ex_{in} is the inlet exergy to the system and function of the sun's outer surface temperature ($T_s = 5800$ K) and defined as Petela [26]:

$$\dot{Ex}_{in} = A_{ap,t} G_b \left(1 + \frac{1}{3}\left(\frac{T_o}{T_s}\right)^4 - \frac{4}{3}\left(\frac{T_o}{T_s}\right)\right) \tag{19}$$

The exergetic fuel depletion ratio of a component j is defined as [21]:

$$Y_{d,j} = \frac{Ex_{d,j}}{Ex_{total,in}} \tag{20}$$

The irreversibility ratio of a component j is defined as [21]:

$$Y_{d,j}^* = \frac{Ex_{d,j}}{Ex_{D,total}} \tag{21}$$

Improvement potential of a component j is defined as:

$$IP_j = \left(1 - \frac{\eta_{ex,el}}{100}\right)Ex_{d,j} \tag{22}$$

4. Results and discussion

In designing a solar thermal power plant, the main variable to examine is the variation of solar irradiation on the plant performance. To assess its effect on power plant exergetic performance, variation of the steam turbine inlet pressure is another key variable. Furthermore, investigating the effect of varying the net electrical power output, which in turn affect the solar field size, is another key variable in the exergetic performance of the system. The variation of the net electrical power output in the steam Rankine cycle is attained through varying the mass flow rate of the steam. Therefore, the effects of these three variables on the exergetic performance of the systems considered were examined. The exergetic performance of the systems considered were evaluated, in detail, under solar irradiation intensity – $G_b = 0.8$ kW/m² – as an average peak value in which the thermal power plant is operated. Furthermore, the effect of the solar irradiation during daytime on the systems considered was examined, and a wide range of solar intensity was considered, $G_b = 0.5–0.9$ kW/m². The thermodynamic properties under the baseline conditions for the solar irradiation intensity $G_b = 0.8$ kW/m² case for the three systems are listed in Tables 3–5. As discussed before, the results are presented for three cases, in which all are integrated with the PTSC. These cases are the steam Rankine cycle under vacuum condensing pressure (SRC-V), the steam Rankine cycle under atmospheric condensing pressure (SRC-A), and the combined cycle operated through steam and a refrigerant in which the exit pressure of the steam turbine is atmospheric pressure for the reasons discussed before. For the combined cycles, seven refrigerants were investigated.

4.1. Solar irradiation intensity variation results

Solar irradiation intensity variation effects on the exergetic performance of the system considered is illustrated in Fig. 3–5. Fig. 3 reveals that as the solar irradiation intensity increases, the exergetic efficiencies of the thermal cycles increase. This result can be explained as follows. First, the solar field is designed to work with a specific range of solar collector rows. Second, receiving more solar radiation means better utilization of the available solar collector field, which could result in using fewer numbers of solar collectors. Therefore, as demonstrated in the figure, improvement in the overall exergetic efficiency of the system can be obtained as the thermal irradiation increases. This figure illustrates that the SRC-V has the highest exergetic efficiency while SRC-A has the lowest exegetic efficiency. Among the combined cycles considered, the R134a combined cycle has the highest exergetic efficiency followed by R152a combined cycle, while the R600a combined cycle has the lowest efficiency. Furthermore, this figure shows that the exergetic efficiency of the R134a combined cycle increases from around 23% at $G_b = 0.5–25.5\%$ at $G_b = 0.9$ 5 kW/m² while the R600a combined cycle exergetic efficiency increases from 20.2% to 22.5% as the solar irradiation intensity increases. In addition, it is revealed that the other combined cycles have marginal differences in their exergetic efficiency values.

To further assess the exergetic performance of the cycles considered, total exergy destruction rates of these cycles are demonstrated in Fig. 4. This figure reveals that as the solar irradiation intensity increases, the total exergy destruction rates decrease. This decrement is expected, owing to the increase in the exergetic efficiency as the solar irradiation intensity increases, where the exergetic efficiency is an inverse function of exergy destruction rate as long as the exergy loss is less than the exergy destructed. This figure demonstrates that SRC-A has the largest exergy destruction rate while the R134a combined cycle and SRC-V have the lowest exergy destruction rates. Moreover, R407c, R600, and ammonia combined cycles have marginal differences in their exergy destruction rate values. The exergy destruction rate of the R134a combined cycle decreases from almost 157 MW to 136 MW as the solar irradiation intensity increases while the exergy destruction rate of the SRC-A decreases from around 190 MW to 160 MW as the solar irradiation intensity increases.

The main source of exergy destruction in these cycles is the solar collectors and, hence, it will be significant to examine the

Table 3
Properties of the selected refrigerants [22].

Substance	Physical data				Safety data	Environmental data		
	Molecular mass (kg/kmol)	T_{bp}[a] (°C)	T_{crit}[b] (°C)	P_{crit}[c] (MPa)	ASHRAE 34 safety group	Atmospheric life time (yr)	ODP[d]	GWP[e] (100 yr)
R134a	102.03	−26.1	101	4.059	A1	14	0	1430
R152a	66.05	−24	113.3	4.52	A2	1.4	0	124
R290	44.1	−42.1	96.68	4.247	A3	0.041	0	∼20
R407c	86.2	−43.6	86.79	4.597	A1	n.a.	0	1800
R600	58.12	−0.5	152	3.796	A3	0.018	0	∼20
R600a	58.12	−11.7	135	3.647	A3	0.019 0	0	∼20
R717 (ammonia)	17.03	−33.3	132.3	11.333	B2		0.01	<1

n.a., not-available.
 [a] T_{bp}: normal boiling point.
 [b] T_{crit}: critical temperature.
 [c] P_{crit}: critical pressure.
 [d] ODP: ozone depletion potential, relative to R11.
 [e] GWP: global warming potential, relative to CO_2.

Table 4
Thermodynamic properties of the stations for PTSC and R134a combined vapor cycle.

St#	Fluid type	$\dot{m}$ (kg/s)	P (kPa)	T (K)	h (kg/kg)	ex (kJ/kg)
1	Therminol-VP1	134.8	17,254.1	334.2	557.2	37.5
2	Therminol-VP1	134.8	23,544.7	663.0	1718.1	758.8
3	Therminol-VP1	134.8	17,254.1	334.2	557.2	37.5
4	Steam	61.5	12,000.0	374.3	433.0	46.7
5	Steam	61.5	12,000.0	653.0	2977.2	1204.0
6	Steam	61.5	100.0	372.8	2278.2	406.2
7	Steam	61.5	100.0	372.8	417.5	33.7
8	R134a	591.8	2678.9	309.6	102.8	44.8
9	R134a	591.8	2678.9	362.8	296.1	71.4
10	R134a	591.8	887.5	315.5	277.0	49.0
11	R134a	591.8	887.5	308.2	100.9	43.2
12	Cooling water	2343.0	101.3	298.2	104.8	0.0
13	Cooling water	2343.0	101.3	308.8	149.3	0.8

Table 5
Thermodynamic properties of the stations for PTSC and SRC-V cycle.

St#	Fluid type	m (kg/s)	P (kPa)	T (K)	h (kg/kg)	ex (kJ/kg)
1	Therminol-VP1	131.6	17,254.1	334.2	557.2	37.45
2	Therminol-VP1	131.6	23,544.7	663	1718.1	758.8
3	Therminol-VP1	131.6	17,254.1	334.2	557.2	37.45
4	Steam	54.25	12,000	309.19	161.6	12.73
5	Steam	54.25	12,000	653	2977.2	1204
6	Steam	54.25	5.627	308.15	2000.8	60.76
7	Steam	54.25	5.627	308.15	146.6	0.5903
8	Cooling water	2250	101.3	298.15	104.8	0
9	Cooling water	2250	101.3	308.84	149.5	0.7825

Table 6
Thermodynamic properties of the stations for PTSC and SRC-A cycle.

| St#	Fluid type	m (kg/s)	P (kPa)	T (K)	h (kg/kg)	ex (kJ/kg)
1	Therminol-VP1	167.3	17,254.06	334.2	557.2	37.45
2	Therminol-VP1	167.3	23,544.66	663	1718.1	758.8
3	Therminol-VP1	167.3	17,254.06	334.2	557.2	37.45
4	Steam	76.34	12,000	374.33	433	46.67
5	Steam	76.34	12,000	653	2977.2	1204
6	Steam	76.34	100	372.78	2278.2	406.2
7	Steam	76.34	100	372.78	417.5	33.66
8	Cooling water	3177	101.3	298.15	104.8	0
9	Cooling water	3177	101.3	308.84	149.5	0.7825
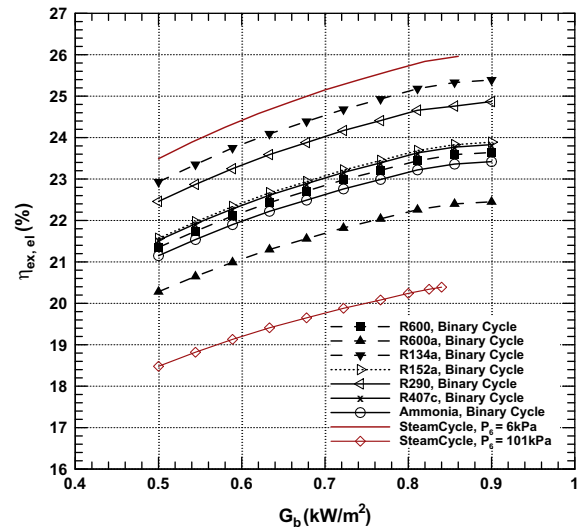
Fig. 3. Electrical exergetic efficiency versus solar irradiation intensity for a net electrical power of 50 MWe.
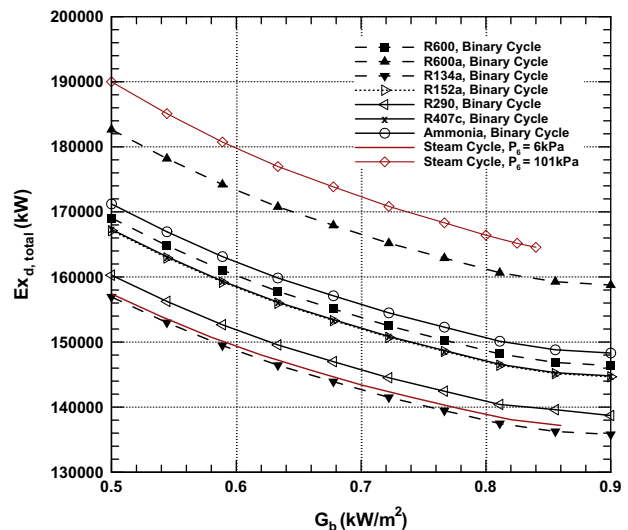

Fig. 4. Total exergy destruction rate versus solar irradiation intensity for a net electrical power of 50 MWe.
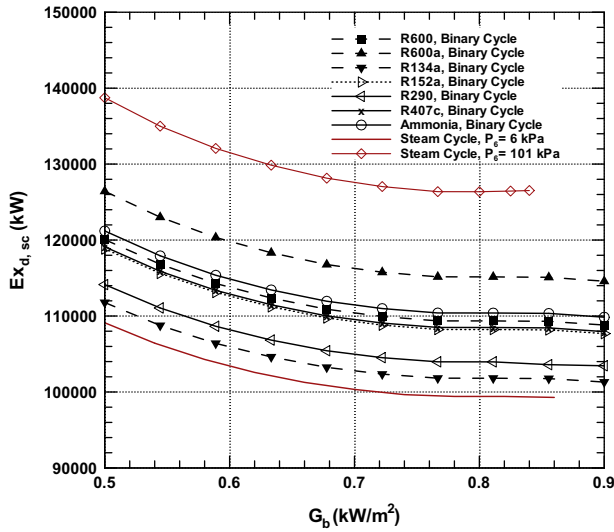
Fig. 5. Solar collector exergy destruction rate versus solar irradiation intensity for a net electrical power of 50 MWe.

exergy destructed due to them. The exergy destruction due to the exergy losses in the solar collector is illustrated in Fig. 5. This figure reveals that as the solar irradiation intensity increases, the exergy destructed by the solar collector field decreases, which is due to the better utilization of the available collectors and using fewer solar collector rows. Note that the solar collector field size is designed with a solar multiple larger than one and, therefore, fewer solar collector rows are used at higher solar irradiation. In addition, this figure illustrates that the maximum exergy destruction rate in these cycles is 139.5 MW at G_b = 139.5 kW/m^2 for the SRC-A while the lowest value is around 100 MW at G_b = 0.9 kW/m^2 for the SRC-V. The other cycles have exergy destruction rates between these two values.

4.2. Net electrical power variation results

In the previous subsection, the considered systems are designed to produce a net electrical power of 50 MW. Therefore, as presented in Fig. 6, it would be beneficial to consider the effect of varying the net electrical power on the exergy destruction rate of the
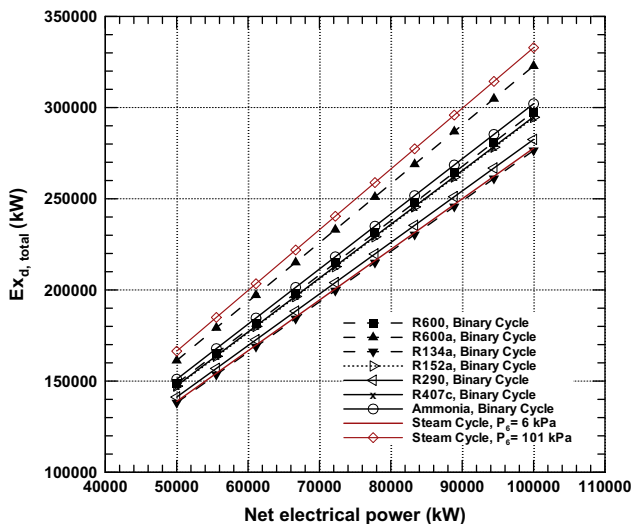
systems considered. It is shown in this figure that as the net electrical power increases, the total exergy destruction rate increases linearly. It is observed that as the net electrical power increases from 50 MW to 100 MW, the total exergy destruction rate increases, on average, by 165 MW. Furthermore, at the net electrical power production of 50 MW, the difference between the minimum and maximum exergy destruction rate for all cycles is around 27 MW while this difference increases to 59 MW at 100 MW. This increment is expected because of the increment in the size of the power plant, especially the solar collector field, due to the increase in the needed electrical power production.

4.3. Steam turbine inlet pressure variation results

Steam turbine input pressure is of significant important in designing combined vapor cycles and, hence, it is being investigated in this study. Figs. 7–9 illustrate the effect of the steam turbine inlet pressure on the exergetic performance of the systems considered. Fig. 7 illustrates the effect of steam turbine inlet pressure on the overall exergetic efficiencies of the systems considered. It is noticed that as the pressure increases, the exergetic efficiencies of all systems increase. This increase in the exergetic efficiencies owes to improvement in the energetic performance of the systems as the pressure increases. It is observed that the exergetic efficiency of the SRC-V is the largest which is around 25% at 8 MPa and increases to 26% at 15 MPa while the exergetic efficiency for the SRC-A is the lowest which is around 19.2% at 8 MPa and increases to 20.6% at 15 MPa. The exergetic efficiency of other cycles is between these values of the two cycles. The R134a combined cycle has the highest exergetic efficiency among the combined cycles considered followed by the R152a combined cycle, whereas the R600a combined cycle has the lowest exergetic efficiency. The other cycles, R600, R290, R407a, and the ammonia combined cycles have comparable exergetic efficiencies attributable to the comparable energetic performance of these cycles.

The effect of steam turbine inlet pressure on the total exergy destruction rate is illustrated in Fig. 8. This figure demonstrates that as this pressure increases, the total exergy destruction decreases. This decrement is attributed to the improvement in the exergetic efficiency as the pressure increases as presented in Fig. 8. This figure demonstrates that the SRC-V and R134a combined cycle have the lowest exergy destruction rate which decreases from approximately 144 MW at 80 MPa to 136 MW at
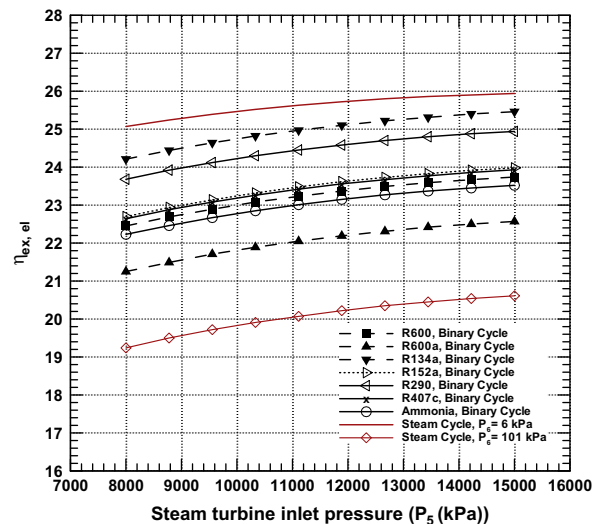

Fig. 6. Total exergy destruction rate versus net electrical power for solar irradiation of G_b = 0.8 kW/m^2.

Fig. 7. Electrical exergy efficiency versus steam turbine inlet pressure for a net electrical power of 50 MWe.
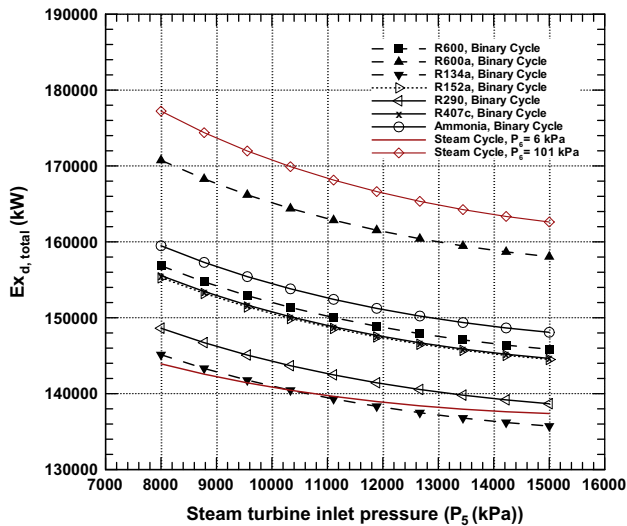
Fig. 8. Total exergy destruction rate versis steam turbine inlet pressure for a net electrical power of 50 MWe.
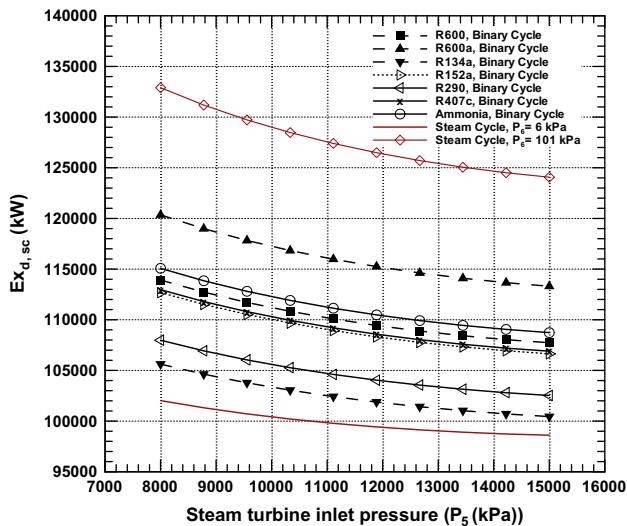

Fig. 9. Solar collector exergy destruction rate versus steam turbine inlet pressure for a net electrical power of 50 MWe.

15 MW. Alternatively, the R600a combined cycle has the highest exergy destruction rate among the combined cycles considered, which is around 171 MW at 8 MPa and decreases to 158 MW at 15 MPa.

Further in-depth analysis of the exergy destruction demonstrates that the main source of the exergy destruction is the solar collectors as illustrated in Fig. 9. It observed that the contribution of the solar collector in exergy destruction could reach 75% which is very large. Therefore, further careful design and improvement is crucial to reduce this loss. For example, the total exergy destruction rate of R600a combined cycle at 8 MPa is 17.5 MW in which 12 MW (from this value) is from the solar collector, which is a significant amount. Similar observations can be noticed for other cycles.

4.4. Detailed exergy analysis of system components results

Detailed exergy analysis was conducted through exergetic assessment of the main components of the systems considered is discussed in this section. The exergetic assessment considered

Table 7
Detailed exergy parameters for R134a combined vapor cycle.

	Ex_d (kW)	IP (kW)	Y_D	Y_D^*
Solar collector	10,1810	76,234	0.512	0.73
Condenser	1616	1210	0.008	0.012
Evaporator	26,055	19,510	0.131	0.18
Heat exchanger	7130	5339	0.036	0.05
ORC pump	218	163.2	0.001	0.002
ORC turbine	1902	1424	0.010	0.014
Solar pump	0.66	0.496	0.000	0.000
Steam pump	151.8	113.6	0.001	0.001
Steam turbine	6068	4544	0.030	0.044
Total	137,822	103,200	0.728	1.0

Table 8
Detailed exergy parameters for SRC-V cycle.

	Ex_d (kW)	IP (kW)	Y_D	Y_D^*
Solar collector–receiver	99,379	73,804	0.512	0.71
Condenser	1504	1117	0.008	0.011
Evaporator	30,288	22,493	0.156	0.218
Solar subsystem pump	0.65	0.48	0.000	0.000
Steam pump	157.6	117	0.001	0.001
Steam turbine	9044	6717	0.047	0.065
Total	138,869	103,131	0.723	1.0

Table 9
Detailed exergy parameters for SRC-A Cycle.

	Ex_d (kW)	IP (kW)	Y_D	Y_D^*
Solar collector-receiver	126,368	100,793	0.512	0.73
Condenser	25,950	20,698	0.105	0.15
Evaporator	32,340	25,795	0.131	0.17
Solar subsystem pump	0.82	0.66	0.000	0.000
Steam pump	188.4	150.3	0.001	0.001
Steam turbine	7532	6008	0.030	0.045
Total	166,429	132,746	0.779	1.0

key exergy parameters including exergy destruction rate, exergetic improvement potential, exergetic fuel depletion ratio, and relative irreversibility as shown in Tables 7–9. The values of these parameters are under the baseline conditions: steam turbine inlet pressure is 12 MPa, $G_b = 0.8$ kW/m², and the net electrical power is 50 MW.

From Table 7, it observed that the main source of exergy destruction is the solar collectors, which is 101,810 kW. The main reason of this large exergy destruction is the large temperature difference in the collector. Other main sources of exergy destruction are the evaporator, at 26,055 kW; then the heat exchanger, at 7130 kW; and the steam turbine, at 6068 kW. All three components are characterized by large temperature differences which causes large exergy destruction. Considering the SRC-V and SRC-A cycles, the main two sources of exergy destruction are the solar collectors and the evaporator, Tables 8 and 9.

Improvement potential is an indicator of possible improvement in the system from an exergetic point of view. As indicated above, the main source of exergy destruction is the solar collector and, thus, it requires careful design to improve its performance. For the R134a combined cycle, the exergy destructed is 101,810 kW while the improvement potential is 76,234 kW as listed in Table 6. This means that around 75% of the destructed exergy could be avoided if a careful and an improved design of the solar collector is conducted. An improved design includes, mainly, higher optical efficiency of the collector and less heat losses from the receiver. The same observations are noticed for other cycles, as indicated in Tables 8 and 9. Another main source of exergy destruction is

the evaporator which accounts for 26 MW in the R134a combined cycle whereas the calculated improvement potential is around 19.5 MW. The main source of this exergy destruction is the temperature difference between the incoming oil, state 2, and the leaving steam, state 5, and, therefore, further improvement can be attained by careful design of the evaporator, which would require a larger heat exchange surface area and, consequently, more cost. The exergetic fuel depletion ratio is a parameter indicating the ratio of the exergy destruction as compared to the inlet exergy. Tables 7–9 show that around half of the inlet exergy is destructed in the solar collectors and 13–15% of it is destructed in the evaporator. Another important observation is for the steam turbine. It is observed that for the R134a combined cycle and SRC-A cycle the fuel depletion is around 3% for the steam turbine while this value is around 4.6% for the SRC-V. This difference in the fuel depletion values indicates that the steam turbine design is more critical for the SRC-V as compared to the other two cycles.

The relative irreversibility is another important exergetic parameter that identifies the ratio of the exergy destructed to the total exergy destructed in a system. Tables 7–9 demonstrate that around 71–73% of the destructed exergy occurs in the solar collectors. It is listed in these tables that the other main source of exergy destruction is the evaporator which accounts for at least 18%.

5. Conclusions

In this study, detailed exergy analysis of the SRC and combined Rankine cycles both integrated with parabolic trough solar collectors was conducted. The study considered seven refrigerants for the bottoming cycle (for the combined cycles cases): R134a, R152a, R290, R407c, R600, R600a, and ammonia. The following can be concluded from this study:

- As the solar irradiation increases, the exergetic efficiency of the systems considered increases.
- The parabolic trough solar collectors are the main source of the exergy destruction in which more than 50% of the solar inlet exergy is destructed which is significant. This value accounts for around 70% of the total exergy destructed. Therefore, there is a significant need for a careful design of the PTSC to reduce the exergy destructed in these components.
- The evaporator is another source of exergy destruction in which around 13% of the solar inlet exergy is destructed. This value accounts for around 19% of the total exergy destructed in the system.
- The overall exergetic improvement potential of the systems considered is around 75%.
- The R134a combined cycle followed by R152a combined cycle demonstrated the best exergetic performance among the combined cycles considered. Alternatively, the R600a combined cycle had the lowest exergetic performance.
- The difference between the exergetic performance of R290, R407c, R600, and ammonia combined cycles was marginal.

Acknowledgement

References

[1] He Ya-Ling, Mei Dan-Hua, Tao Wen-Quan, Yang Wei-Wei, Liu Huai-Liang. Simulation of the parabolic trough solar energy generation system with organic Rankine cycle. Appl Energy 2012;97:630–41.
[2] Quoilin S, Orosz M, Hemond H, Lemort V. Performance and design optimization of a low-cost solar organic Rankine cycle for remote power generation. Sol Energy 2011;85:955–66.
[3] Bamgbopa MO, Uzgoren E. Quasi-dynamic model for an organic Rankine cycle. Energy Convers Manage 2013;72:117–24.
[4] Gang Pei, Li Jing, Jie Ji. Analysis of low temperature solar thermal electric generation using regenerative organic Rankine cycle. Appl Therm Eng 2010;30:998–1004.
[5] Jing Li, Gang Pei, Jie Ji. Optimization of low temperature solar thermal electric generation with organic Rankine cycle in different areas. Appl Energy 2010;87:3355–65.
[6] Derscha Jurgen, Geyer Michael, Herrmann Ulf, Jones Scott A, Kelly Bruce, Kistner Rainer, et al. Trough integration into power plants—a study on the performance and economy of integrated solar combined cycle systems. Energy 2004;29:947–59.
[7] Li C, Kosmadakis G, Manolakos D, Stefanakos E, Papadakis G, Goswami DY. Performance investigation of concentrating solar collectors coupled with a transcritical organic Rankine cycle for power and seawater desalination co-generation. Desalination 2013;318:107–17.
[8] Nafey AS, Sharaf MA. Combined solar organic Rankine cycle with reverse osmosis desalination process: energy, exergy, and cost evaluations. Renew Energy 2010;35:2571–80.
[9] Sharaf MA, Nafey AS, García-Rodríguez Lourdes. Exergy and thermo-economic analyses of a combined solar organic cycle with multi-effect distillation (MED) desalination process. Desalination 2011;272:135–47.
[10] Delgado-Torres AM, García-Rodríguez Lourdes. Preliminary design of seawater and brackish water reverse osmosis desalination systems driven by low-temperature solar organic Rankine cycles (ORC). Energy Convers Manage 2010;51:2913–20.
[11] Delgado-Torres AM, García-Rodríguez Lourdes. Analysis and optimization of the low-temperature solar organic Rankine cycle (ORC). Energy Convers Manage 2010;51:2846–56.
[12] Al-Sulaiman Fahad A, Hamdullahpur Feridun, Dincer Ibrahim. Performance assessment of a novel system using parabolic trough solar collectors for combined cooling, heating, and power production. Renew Energy 2012;48:161–72.
[13] Al-Sulaiman Fahad A, Dincer Ibrahim, Hamdullahpur Feridun. Exergy modeling of a new solar driven trigeneration system. Sol Energy 2011;85:2228–43.
[14] Al-Sulaiman Fahad A. Energy and sizing analyses of parabolic trough solar collector integrated with steam and binary vapor cycles. Energy 10.1016/j.energy.2013.05.020. [in press].
[15] Montes MJ, Abánades A, Martínez-Val JM. Performance of a direct steam generation solar thermal power plant for electricity production as a function of the solar multiple. Sol Energy 2009;83:679–89.
[16] Zarza E, Rojas ME, González L, Caballero JM, Rueda F. INDITEP: The first pre-commercial DSG solar power plant. Sol Energy 2006;80:1270–6.
[17] LUZ International Limited. Solar electric generating system IX technical description. LUZ International Limited; 1990.
[18] Therminol Heat Transfer Fluids by Solutia Inc. Therminol VP-1, http://www.therminol.com/pages/products/vp-1.asp; 2012.
[19] Price H, Lüpfert E, Kearney D, Zarza E, Cohen G, Gee R, et al. Advances in parabolic trough solar collectors technology. ASME, J Sol Energy 2002;124:109–25.
[20] Valenzuela Loreto, Zarza Eduardo, Berenguel Manuel, Camacho Eduardo F. Control concepts for direct steam generation in parabolic troughs. Sol Energy 2005;78(2):301–11.
[21] Bejan A, Tsatsaronis G, Moran M. Thermal design and optimization. John Wiley and Sons, Inc.; 1996.
[22] Tchanche Bertrand Fankam, Papadakis George, Lambrinos Gregory, Frangoudakis Antonios. Fluid selection for a low-temperature solar organic Rankine cycle. Appl Therm Eng 2009;29(11–12):2468–76.
[23] Kalogirou S. Solar energy engineering: processes and systems. Elsevier; 2009.
[24] Duffie J, Beckman W. Solar engineering of thermal processes. John Wiley & Sons, Inc.; 2006.
[25] Dudley VE, Koib GJ, Mahoney AR, Mancini TR, Matthews CW, Sloan M, Keamey D. SEGS LS-2 solar collector test results. Report of Sandia National Laboratories, SANDIA94-1884; 1994.
[26] Petela R. Exergy analysis of the solar cylindrical-parabolic cooker. Sol Energy 2005;79(3):221–33.
[27] NREL. Heat transfer analysis and modeling of a parabolic trough solar receiver implemented in EES, NREL; 2003.